VII International Conference on Computational Methods for Coupled Problems in Science and Engineering
COUPLED PROBLEMS 2017
M. Papadrakakis, E. Oñate and B. Schrefler (Eds)

TRANSIENT MODELLING OF THE ROTOR-TOWER INTERACTION OF WIND TURBINES USING FLUID-STRUCTURE INTERACTION SIMULATIONS

G. SANTO [1]*, M. PEETERS [2], W. VAN PAEPEGEM [2], J. DEGROOTE [1]

[1] Department of Flow, Heat and Combustion Mechanics, Ghent University
Sint-Pietersnieuwstraat 41 – 9000 Ghent, Belgium
{gilberto.santo; joris.degroote}@ugent.be

[2] Department of Materials, Textiles and Chemical Engineering, Ghent University
Technologiepark-Zwijnaarde 907 – 9052 Zwijnaarde, Belgium
{mathijs.peeters; wim.vanpaepegem}@ugent.be

Key words: Fluid-structure interaction, wind energy, composite materials, atmospheric boundary layer.

Abstract. In this work, we focus on the effect of supporting structures on the loads acting on a large horizontal axis wind turbine. The transient fluid-structure interaction (FSI) is simulated by an in-house code which couples two solvers, one for the computational fluid dynamics (CFD) and one for the computational structure mechanics (CSM). Strong coupling is applied as the force and displacement equilibriums are always enforced on the fluid-structure interface.

The flexibility of the three blades of the considered machine is taken into account. The accurate CSM model reproduces in details the composite layups, foam, adhesive and internal stiffeners of the blades. On the other hand, the supporting structures (tower and nacelle) are considered to be rigid.

On the fluid side, a fully hexahedral mesh is generated by a multi-block strategy. The same mesh is continuously deformed and adapted according to the displacement of the fluid-structure interface. The atmospheric boundary layer (ABL) under neutral conditions is included and consistently preserved along the computational domain.

Using the outlined model, the blade deflections with and without supporting structure are compared. The effects of this transient interaction are highlighted throughout the rotation of the rotor, in terms of both wind energy conversion performance of the machine and structural response of each component. The maximal stress in the blade material as a function of time is compared with and without the presence of the tower in the wake of the rotor. Only a few similar works are reported to appear in literature [1, 2], whereas none of them currently includes the ABL or show detailed information about the internal stresses in the composite blades.

1 INTRODUCTION

The actual tendency of increasing the size of the horizontal axis wind turbine's rotor [3] to maximize the captured energy, and the resulting higher slenderness of their blades, have strengthened the necessity to investigate the mutual interaction of wind flow and structural response of the blades. Previous research has shown that the axial deflection of the blade tips can reach peaks of 10-15% of their total span [4, 5]. As a consequence, the deformed shape of the blades influences the wind flow around them, which in turn affects the structural deflection. This results in a fully coupled problem which is important to take into account in several processes such as design and maintenance estimation of modern horizontal axis wind turbines (HAWTs) [6].

Both sides of this problem, namely the fluid and the structural ones, involve a large complexity when it comes to numerical analysis. On the structural side, the blades' inner and outer structures are made of anisotropic composite material and assembled by means of adhesive joints [7]. On the fluid side, the Reynolds number of the flow can go up to 10^8. The consequent high turbulence levels, combined with the rotation of the blades, make the problem even harder to tackle [2, 4, 5]. Additionally, large HAWTs normally are immersed in the atmospheric boundary layer (ABL) which leads to variable velocity and turbulence in altitude [8]. The presence of the supporting structures (tower and nacelle) represents a disturbance for the flow around the blades passing in their region of influence [1]. This effect, addressed as rotor-tower interaction, is here investigated.

The present work aims at simulating the fully coupled fluid-structure interaction (FSI) problem on a full scale 100m diameter HAWT employing accurate flow and structural models, leading to a fully coupled FSI model. The ABL is also taken into account. The effect of the rotor-tower interaction is highlighted by comparison of results obtained simulating only the rotating parts of the considered HAWT ("rotor only") and results obtained including the supporting structures ("full machine"). On the structural side, a complete and accurate model reproducing the complex composite nature of each blade is built and employed. The implicit coupling between the flow and the structural models is guaranteed by the in-house code Tango, resulting in a partitioned approach [12].

2 METHODOLOGY

The details of the computational fluid dynamics (CFD) and computational structural mechanics (CSM) are now discussed.

2.1 The CFD model

The adoption of different reference frames is necessary: a stationary and a rotating domain are created and separated by sliding interfaces. The layout of the complete mesh is displayed in fig. 1, together with the distances (in terms of turbine diameter D) of the boundaries from the rotating domain and the boundary conditions used.

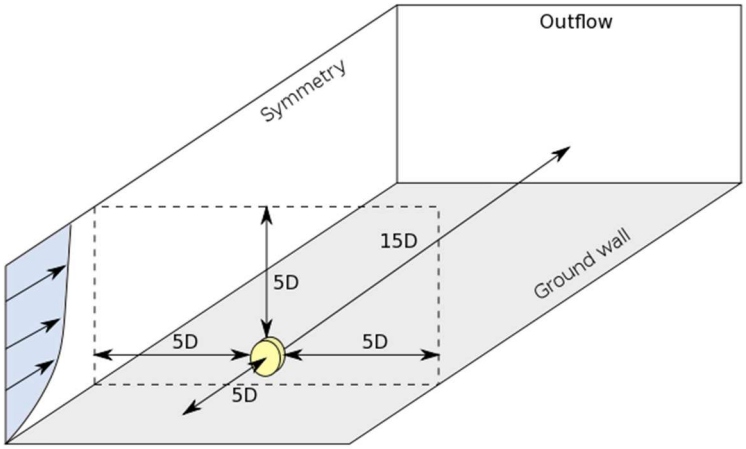

Figure 1: Layout adopted for the HAWT simulations; in yellow, the rotating domain.

Both the "rotor only" (RO) and "full machine" (FM) configurations are displayed in fig. 2. The exact same rotating cylinder is used in both cases while, in the FM case, the stationary domain is adapted to accommodate the supporting structures (tower and nacelle). The tower geometry is chosen to be suitable for the size of the considered HAWT and extracted from [13].

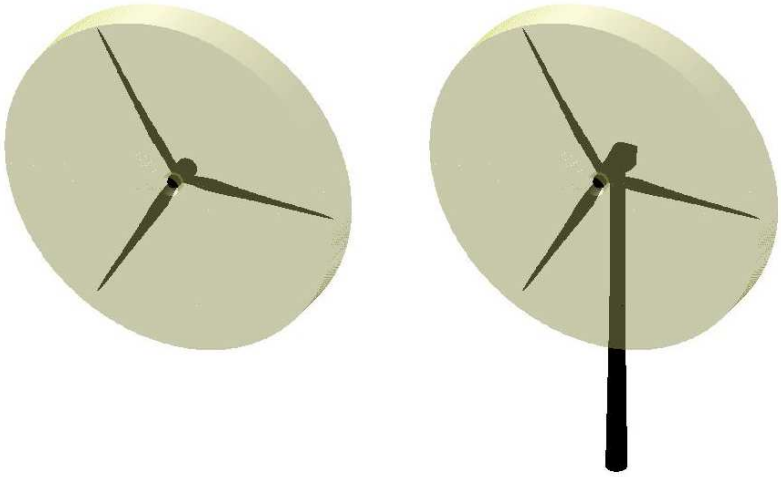

Figure 2: Detail of the rotating domain: (left) RO case and (right) FM case.

Given the low Mach number, the flow is considered incompressible and the turbulence model is chosen to be the $k-\varepsilon$ (unsteady RANS) model, which adds two transport equations.

The ABL inlet conditions first proposed by Richard and Hoxey [8] are employed at the inlet of the stationary domain to replicate the neutral ABL velocity and turbulence stratification. With z the height of the domain (distance from the ground wall), the inlet conditions for velocity u, turbulent kinetic energy k and turbulent dissipation rate ε are

respectively:

$$u(z) = \frac{u_*}{\mathrm{K}} ln\left(\frac{z + z_0}{z_0}\right)$$
$$k = \frac{u_*^2}{\sqrt{C_\mu}}$$
$$\varepsilon(z) = \frac{u_*^3}{\mathrm{K}(z + z_0)}$$

In these equations, u_* represents the friction velocity, an index of the global wind intensity, and z_0 is the aerodynamic roughness length which provides a measure of how rough the ground wall is. In this work, u_* and z_0 are chosen respectively equal to $0.792\ m/s$ and $0.5\ m$, reproducing a rather intense wind over a rough ground. K represents the von Karman constant (0.4187), while C_μ is a constant of the $k-\varepsilon$ model equal to 0.09. In order to guarantee that the imposed inlet profiles are consistently preserved throughout the computational domain, a specific formulation of the wall functions for the ground wall is necessary, according to what was observed by Blocken et al [9] and Parente et al. [10, 11]. Therefore, following what proposed by Parente and Benocci [10], the aerodynamic roughness length is directly included in the ground wall functions, leading to a modified non-dimensional wall distance z^+ and a modified wall function constant E.

$$z^+_{mod} = \frac{(z + z_0)u_*\rho}{\mu}$$
$$E_{mod} = \frac{\mu}{\rho z_0 u_*}$$

On the walls belonging to the wind rotor and the supporting structures, the standard wall functions are employed. The velocity contours are shown in fig. 3, during the FSI simulation with supporting structures. They show clearly the ABL stratification and the recovery of the undisturbed flow conditions beyond the wake of the analyzed machine.

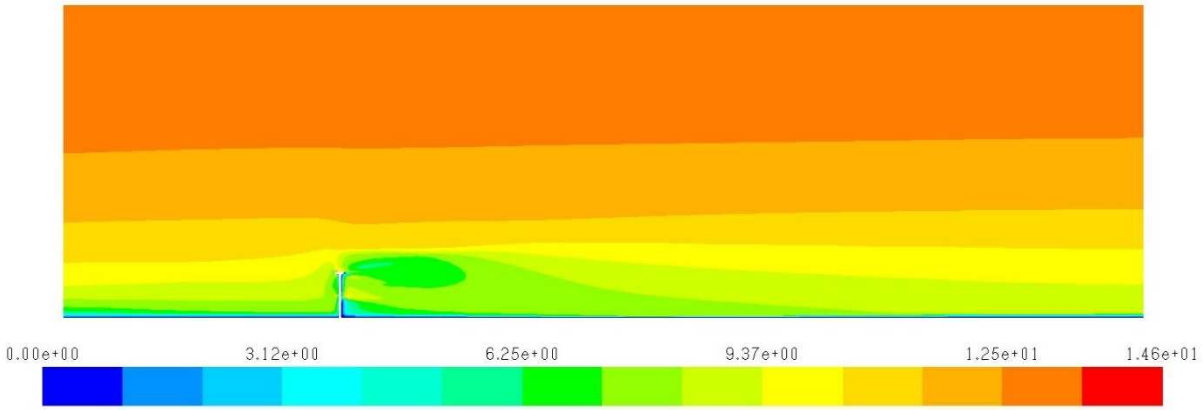

Figure 3: Contours of velocity magnitude (m/s) during FSI-FM simulation.

The mesh is fully hexahedral and built by means of a multi-block strategy. 3 million cells

compose the rotating domain, while the stationary one, is made of 10 million in the RO configuration and 12 million in the FM configuration. Fig. 4 shows two sections of the mesh around a blade, one close to its root and one close to its tip.

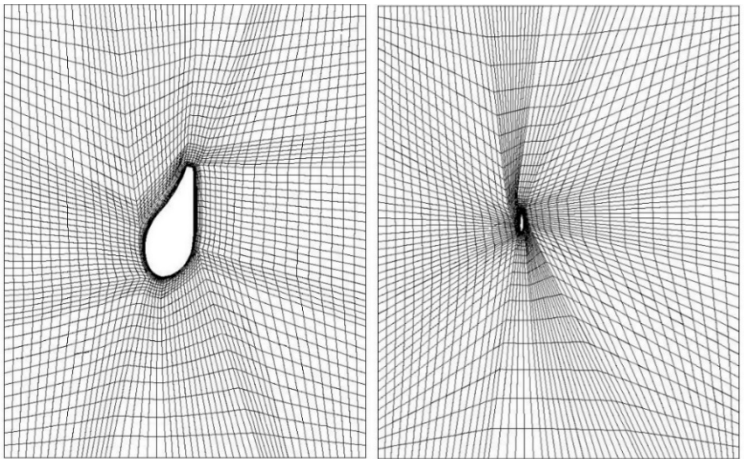

Figure 4: Sections of the mesh around one blade: (left) 20% of the total span and (right) 99% of the total span.

The momentum equations and pressure-based continuity equation are solved together with implicit coupling. 2nd order upwind discretization for momentum is applied and a 2nd order implicit scheme is used for time discretization.

During the FSI simulations, the mesh is adapted only in the rotating domain (fig. 2) in order to allow deformation of the blades as prescribed by the structural solver. The supporting structures are considered to be rigid. A diffusion method based on boundary distance is employed to handle the mesh motion. The need to always preserve the shape of the sliding interfaces translates directly into boundary conditions for the diffusion method.

2.2 The CSM model

The turbine to be analyzed features three $50\,m$ long blades entirely made of composite material. Each blade has a weight exceeding $9\,tons$ and encompasses three shear webs covering a large portion of its span. Shell elements with 3 or 4 nodes and reduced integration are exclusively employed and composite layups are defined to reproduce the composite layering. The elements are positioned on the outer mold layer (OML) with material offset towards the inside, mimicking the blades manufacturing process and maintaining the correct outer blade shape to facilitate the FSI coupling with the CFD model. Different layups are assigned to different regions of the structure, modelling its real composition. A local reference frame is discretely defined in every element in order to fix the global orientation of the layup. In every element, all the layups are then composed of a varying number of plies ranging from 1 to 127. For each ply a material and a thickness are assigned, together with a relative orientation in the form of a rotation angle with respect to the global layup orientation. The shear webs, the shear caps and the adhesive joints are also included. The mesh is created following the process discussed in [14], resulting in a total of 64000 three-dimensional shell elements. The outer structure and the inner shear webs are displayed in fig. 5.

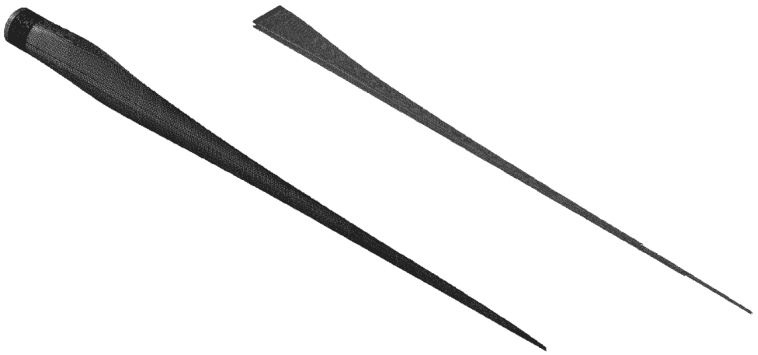

Figure 5: Structural mesh: (left) outer structures and (right) inner shear webs.

During the time span of the simulations, the rotational speed of the machine is fixed at the root of each blade, where all the other degrees of freedom are constrained. The gravity force is also included and accounted for in each simulation.

2.3 FSI coupling

The CFD and the CSM models previously outlined are coupled by means of an in-house code, named Tango [12]. Gauss-Seidel is chosen as coupling algorithm and 3 iterations are performed within every time step, leading to displacement residuals in the order of $3e-2\ m$.

The rotational speed of the turbine is set to $1.3\ rad/s$ which, combined with a wind velocity of $10\ m/s$ at the hub height ($100\ m$) leads to a tip speed ratio λ equal to 6.5. The time step size is chosen to be $0.0403\ s$.

3 RESULTS

In this section the results of various FSI simulations are outlined and compared. Every time-dependent simulation is started from the result of a steady state frozen rotor simulation. In this section, the notation of fig. 6 is used to define the azimuth angle of each blade and the sign of radial and tangential forces and velocities.

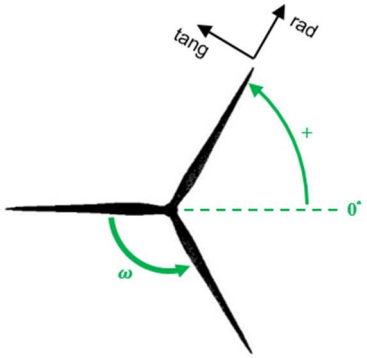

Figure 6: Notation for azimuth angle and components of forces and velocities.

Furthermore the torque (T) and the forces (F) acting on the blades are made non-dimensional by the following formulas:

$$c_T = \frac{T}{\frac{1}{2}\rho v^2 AR}$$
$$c_F = \frac{F}{\frac{1}{2}\rho v^2 A}$$

where $\boldsymbol{\rho}$ is the air density, $\boldsymbol{A}$ the frontal area of the rotor and $\boldsymbol{R}$ its radius; the reference velocity $\boldsymbol{v}$ is chosen to be the free-stream wind velocity at the hub height, namely $\mathbf{10}\ \boldsymbol{m/s}$.

3.1 Rotor only simulations

Starting from a steady state frozen rotor FSI simulation, a first transient FSI simulation is run including only the rotor structures and no supporting structure. The calculation is carried out for two complete revolutions of the rotor. The evolution of the total torque provided by the wind flow to the machine is depicted in fig. 7.

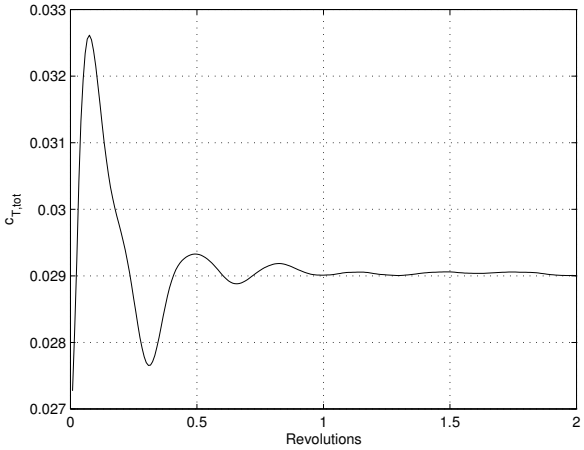

Figure 7: Total torque evolution, RO configuration.

The torque contribution of each blade can be related to its azimuth angle as shown in fig. 8.

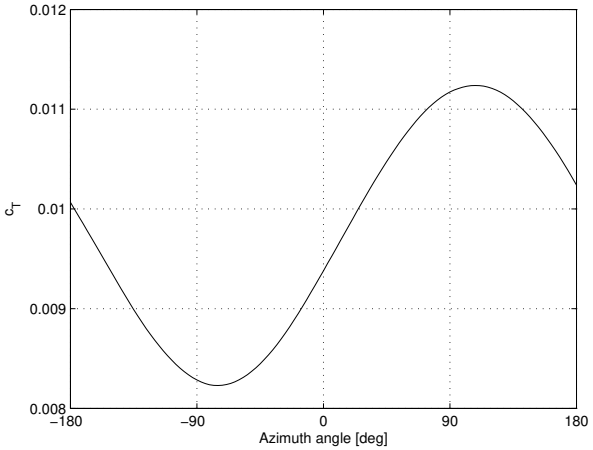

Figure 8: Single blade contribution to the torque, RO configuration.

Fig. 8 clearly shows the effect of the velocity stratification induced by the ABL: for positive azimuth angles, the higher wind velocity induces higher angles of attack on the blade span resulting in higher torque.

In terms of axial force acting on the blade, the same pattern is found. Fig. 9 shows the axial force oscillation during a full revolution, together with the consequent axial displacement of the blade tip.

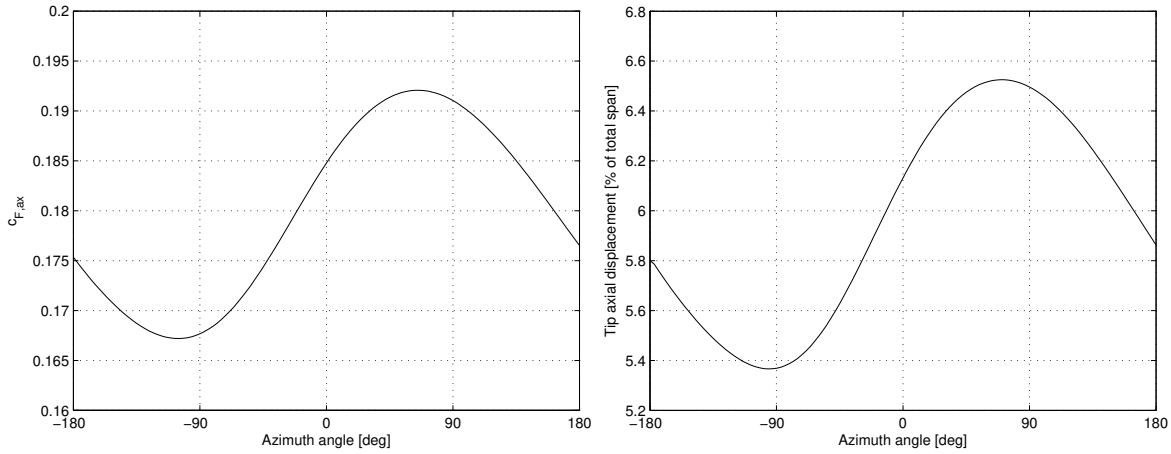

Figure 9: (left) axial force acting on the blade and (right) its axial tip displacement, RO configuration.

It should be noted that the axial force is again higher when the incoming wind velocity is higher, as already observed and commented for the torque. The axial displacement closely follows the oscillation of the axial force and has a mean value of approximately 2.9 m. Fig. 10 shows the deflection of the blade at an azimuth angle of 90 deg.

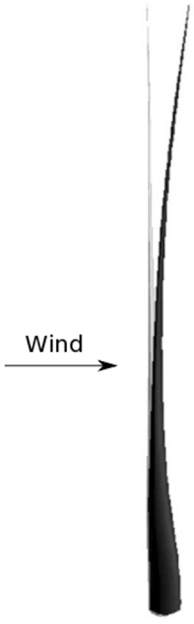

Figure 10: Deformed blade (black) on top of undeformed one (grey), RO configuration.

3.2 Full machine simulations and comparison

The same transient FSI simulation is carried out including the supporting structures and leading to the full machine (FM) configuration. Due to unexpected problems in the mesh motion, only half of a revolution could be simulated. Nevertheless, the passage of the blade in front of the tower was simulated and can be analyzed and compared to the correspondent time span in the RO simulation.

The torque contribution of the blade passing in front of the tower is shown in fig. 11.

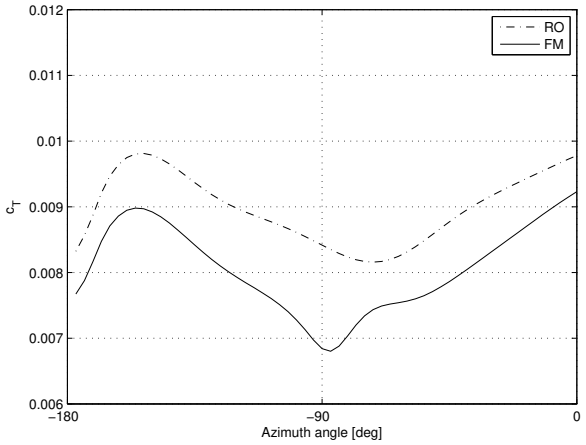

Figure 11: Single blade contribution to the torque, RO vs FM.

It can be seen that the torque provided by the blade is consistently lower (about 5%) in the FM case, compared to the RO configuration. Furthermore, the passage in the front of the tower induces a further drop (5%) which is immediately recovered few degrees later. The tower represents an obstruction and the pressure in the blade-tower clearance is higher than the pressure in the rest of the rotor wake. For this reason, the pressure difference between pressure and suction sides of the blades drops and drags the torque down. This is confirmed by fig. 12 which shows the axial force on the blade as a function of the azimuth angle.

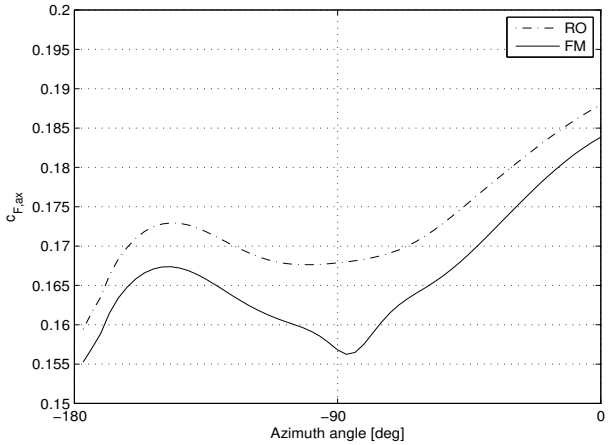

Figure 12: Axial force acting on the blade, RO vs FM.

The torque contribution of each blade can be interpreted as the product of the total tangential force multiplied by the radial position of the center of pressure along the blade span, both shown in fig. 13.

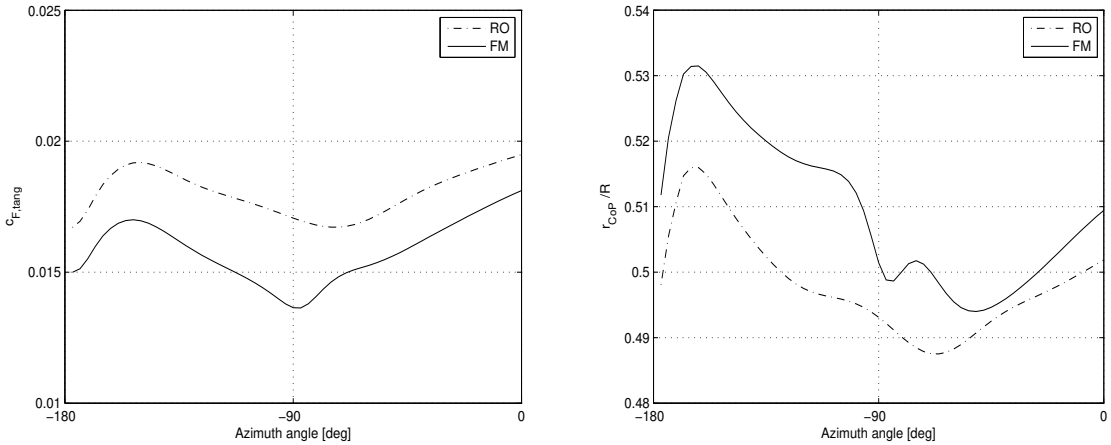

Figure 13: (left) tangential force acting on the blade and (right) relative radial position of the center of pressure, RO vs FM.

The presence of the supporting structures leads to a tangential force consistently lower while the center of pressure is moved towards the tip of the blade due to the presence of the nacelle which reduces the efficiency of the root sections. According to fig. 11, the first effect prevails over the second leading to a lower torque. Splitting the blade into 10 strips, fig. 14 shows the contribution to the torque of each strip at an azimuth angle of $-90\ deg$ for both RO and FM configurations, highlighting how the influence of the tower reduces the torque provided on the entire blade span.

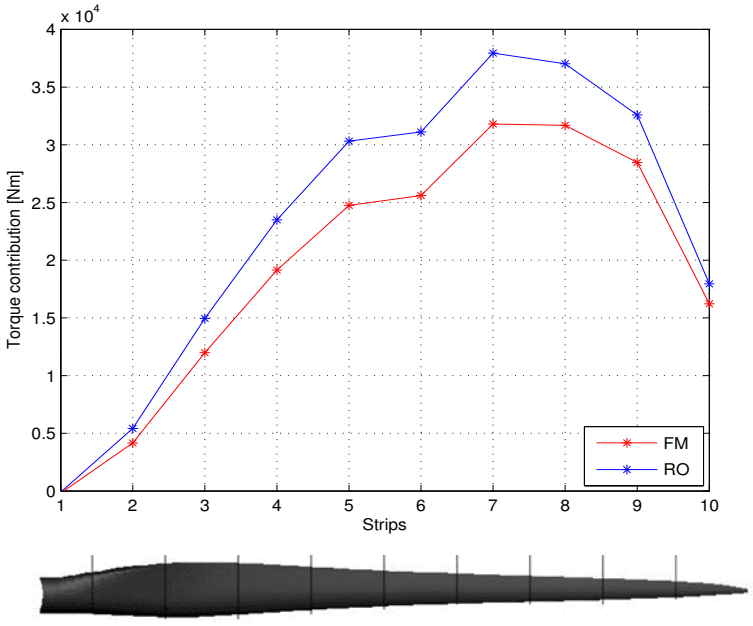

Figure 14: Torque contribution of blade strips, RO vs FM.

4 CONCLUSIONS

The FSI model could be used to investigate the effect of the supporting structures on the performance and loads of a modern HAWT. A drop is observed when the blade passes in front of the tower. The total drop appears to be equally distributed over the entire blade span. At the same time, the axial force transmitted to the blade by the wind is reduced due to the passage in the region of influence of the tower.

Due to unforeseen difficulties in the mesh motion, only half of a complete revolution could be simulated in the full machine configuration. Simulating longer will provide additional insights and details on the investigated phenomenon.

REFERENCES

[1] MC. Hsu, Y. Bazilevs. "Fluid–structure interaction modeling of wind turbines: simulating the full machine". *Computational Mechanics* 2012. DOI: 10.1007/s00466-012-0772-0.

[2] Y. Bazilevs, A. Korobenko, X. Deng, J. Yan, "Novel structural modeling and mesh moving techniques for advanced fluid-structure interaction simulation of wind turbines". *International Journal for Numerical Methods in Engineering* 2015. DOI: 10.1002/nme.4738.

[3] M. Caduff, M.A.J. Huijbregts, H.J. Althaus, A. Koehler, S. Hellweg. "Wind power electricity: the bigger the turbine, the greener the electricity?" *Environmental Science & Technology* 2012. DOI: 10.1021/es204108n

[4] Y. Bazilevs, M.C. Hsu, I. Akkerman, S. Wright, K. Takizawa, B. Henicke, T. Spielman, T.E. Tezduyar. "3D simulation of wind turbine rotors at full scale. Part I: Geometry modeling and Aerodynamics". *International journal for numerical methods in fluids* 2010. DOI: 10.1002/fld.2400

[5] Y. Bazilevs, M.C. Hsu, I. Akkerman, S. Wright, K. Takizawa, B. Henicke, T. Spielman, T.E. Tezduyar. "3D simulation of wind turbine rotors at full scale. Part II: Fluid–structure interaction modeling with composite blades". *International journal for numerical methods in fluids* 2010. DOI: 10.1002/fld.2400

[6] E. Hau. "Wind Turbines: fundamentals, Technologies, Application, Economics" (2nd Edition). *Springer: Berlin*, 2006

[7] YJ Lee, YT Jhan, CH Chung. "Fluid–structure interaction of FRP wind turbine blades under aerodynamic effect". *Composites Part B: Engineering* 2012. ISSN 1359-8368.

[8] P.J. Richards, R.P. Hoxey. "Appropriate boundary conditions for computational wind engineering models using the k-ε turbulence model". *Journal of Wind Engineering and Industrial Aerodynamics* 1993, 46 & 47, 145-153.

[9] Blocken B, Stathopoulos T, Carmeliet J. "CFD simulation of the atmospheric boundary layer: wall function problems". *Atmospheric Environment* 2007. 41:238–252

[10] A. Parente, C. Gorlé, J. van Beeck, C. Benocci. "A Comprehensive Modelling Approach for

the Neutral Atmospheric Boundary Layer: Consistent Inflow Conditions, Wall Function and Turbulence Model". *Boundary Layer Meteorology* 2011. DOI 10.1007/s10546-011-9621-5.

[11] A. Parente, C. Gorlé, J. van Beeck, C. Benocci. "Improved k–e model and wall function formulation for the RANS simulation of ABL flows". *Journal of Wind Engineering and Industrial Aerodynamics* 2011. DOI: 10.1016/j.jweia.2010.12.017.

[12] J. Degroote. "Partitioned simulation of fluid-structure interaction: Coupling black-box solvers with quasi-Newton techniques". *Archives of Computational Methods in Engineering* 2013. DOI: 10.1007/s11831-013-9085-5.

[13] R. Harte, G. Van Zijl. "Structural stability of concrete wind turbines and solar chimney towers exposed to dynamic wind action". *Journal of Wind Engineering* 2007. DOI: 10.1016/j.jweia.2007.01.028.

[14] M. Peeters , W. Van Paepegem. "Development of automated high fidelity finite element models for large wind turbine blades". *16th European Conference on Composite Materials*, Seville, Spain, 22-26 June 2014.